A Peptide-Coated Gold Nanocluster Exhibits Unique Behavior in Protein Activity Inhibition

ARTICLE *in* JOURNAL OF THE AMERICAN CHEMICAL SOCIETY · JUNE 2015

Impact Factor: 12.11 · DOI: 10.1021/jacs.5b00888 · Source: PubMed

6 AUTHORS, INCLUDING:

Deyi An
Chinese Academy of Sciences
3 PUBLICATIONS **4** CITATIONS
SEE PROFILE

Xueyun Gao
Chinese Academy of Sciences
84 PUBLICATIONS **2,923** CITATIONS
SEE PROFILE

Jingyuan Li
Chinese Academy of Sciences
49 PUBLICATIONS **1,106** CITATIONS
SEE PROFILE

JACS
JOURNAL OF THE AMERICAN CHEMICAL SOCIETY

Article

pubs.acs.org/JACS

A Peptide-Coated Gold Nanocluster Exhibits Unique Behavior in Protein Activity Inhibition

Deyi An,[†,‡] Jiguo Su,[‡] Jeffrey K. Weber,[§] Xueyun Gao,[†] Ruhong Zhou,*[,§,∥,⊥] and Jingyuan Li*[,†]

[†]CAS Key Lab for Biomedical Effects of Nanomaterials and Nanosafety, Institute of High Energy Physics, Chinese Academy of Science, Beijing 100049, PR China

[‡]College of Science, Yanshan University, Qinhuangdao 066004, PR China

[§]IBM Thomas J. Watson Research Center, Yorktown Heights, New York 10598, United States

[∥]Institute of Quantitative Biology and Medicine, SRMP and RAD-X, Soochow University, Suzhou 215123, PR China

[⊥]Department of Chemistry, Columbia University, New York, New York 10027, United States

Supporting Information

ABSTRACT: Gold nanoclusters (AuNCs) can be primed for biomedical applications through functionalization with peptide coatings. Often anchored by thiol groups, such peptide coronae not only serve as passivators but can also endow AuNCs with additional bioactive properties. In this work, we use molecular dynamics simulations to study the structure of a tridecapeptide-coated Au_{25} cluster and its subsequent interactions with the enzyme thioredoxin reductase 1, TrxR1. We find that, in isolation, both the distribution and conformation of the coating peptides fluctuate considerably. When the coated AuNC is placed around TrxR1, however, the motion of the highly charged peptide coating (+5e/peptide) is quickly biased by electrostatic attraction to the protein; the asymmetric coating acts to guide the nanocluster's diffusion toward the enzyme's negatively charged active site. After the AuNC comes into contact with TrxR1, its peptide corona spreads over the protein surface to facilitate stable binding with protein. Though individual salt bridge interactions between the tridecapeptides and TrxR1 are transient in nature, the cooperative binding of the peptide-coated AuNC is very stable, overall. Interestingly, the biased corona peptide motion, the spreading and the cooperation between peptide extensions observed in AuNC binding are reminiscent of bacterial stimulus-driven approaching and adhesion mechanisms mediated by cilia. The prevailing AuNC binding mode we characterize also satisfies a notable hydrophobic interaction seen in the association of thioredoxin to TrxR1, providing a possible explanation for the AuNC binding specificity observed in experiments. Our simulations thus suggest this peptide-coated AuNC serves as an adept thioredoxin mimic that extends an array of auxiliary structural components capable of enhancing interactions with the target protein in question.

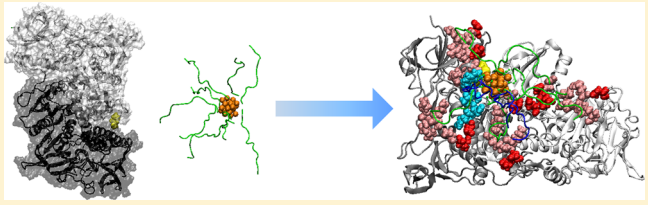

INTRODUCTION

Gold nanoparticles, including nanocrystals and nanoclusters, exhibit great potential in drug delivery, diagnostic, and therapeutic applications within a wide range of biomedical fields.[1−3] In order to improve the stability of particulate suspensions, gold nanoparticles are often protected with various synthetic or biologically inspired coatings composed of alkanethiols, DNAs, or peptides.[4−6] Incidentally, such coatings have also been found to modulate the surface properties and reduce the potential cytotoxicity of the underlying gold nanoparticles.[7,8] Peptide-protected gold nanoparticles, in particular, have received growing attention in recent years.[9−13] Peptide coatings can not only bestow remarkable biocompatibility upon nanoparticle systems, but also endow such nanoparticles with biologically specific functionalities.[14−20] For example, gold nanoparticles conjugated with designed peptide sequences can be used to target and bind disease-related proteins of interest, serving as molecular probes for diagnosis as well as therapeutic agents.[15] Furthermore, conjugated peptides can facilitate the transportation of gold nanoparticles through cell membranes.[18]

Molecular dynamics (MD) simulations have been previously used to study the properties of coated gold nanoparticles. For example, alkanethiol coatings have been found to favor an asymmetric distribution on their gold nanoparticle substrates that results in anisotropic self-assembly on the mesoscale.[21−23] Furthermore, the adsorption of similar nanoparticles onto lipid bilayers and a resultant disruption of bilayer structure have been characterized.[24,25] The structural[26] and self-assembly[27] properties of DNA-coated gold nanoparticles have also been probed using molecular simulation techniques, as well as the impact of DNA coatings on their interactions with cell membranes.[28] Despite the aforementioned applicability of peptide-coated gold nanoparticles, however, little computational data relevant to these peptide-coated systems exist, to our knowledge. Though

Received: January 27, 2015

DOI: 10.1021/jacs.5b00888
J. Am. Chem. Soc. XXXX, XXX, XXX−XXX

interactions between gold nanoparticles and proteins have been explored using computational means, most studies are restricted to the bare nanoparticles.[29,30] The molecular and mechanistic details concerning how peptide- or protein-coated gold nanoparticles interact with proteins, thus, remain to be elucidated.

Thioredoxin reductase 1 (TrxR1), an enzyme that catalyzes disulfide bond cleavage within the antioxidant protein thioredoxin, is known to play an important role in the regulation of cellular redox levels and the growth of tumors.[31,32] And TrxR1 has become an important target for the development of antitumor therapeutic agents.[33,34] Several gold-containing compounds have been designed to inhibit the activity of TrxR1, leveraging coordination between gold atoms and the SH/SeH groups in the active site of TrxR1.[35,36] Systemically, reductions in TrxR1 activity can result in increased concentrations of reactive oxygen species, in principle promoting apoptosis in tumor cells. Recently, our collaborators synthesized a peptide-coated gold nanocluster, Au_{25}peptide$_9$, comprised of a 25 gold atom-core coated with nine tridecapeptides.[37] The conjugated peptides are highly positively charged (+5e), an important property for ensuring favorable solubility and the ease of membrane translocation. Interestingly, this peptide-coated gold nanocluster (AuNC) has been shown to effectively bind and inhibit TrxR1, inducing tumor cell apoptosis in a dose dependent manner.[38]

In this work, we employ MD simulations[39−44] to study the structure and dynamics of these peptide-coated AuNCs in solution and in interaction with TrxR1. We find that the high charge (and concomitant common repulsion) shared among the tridecapeptides is insufficient to overcome the configurational entropy within the coating's structural ensemble: the peptide corona assumes a largely disordered and fluctuating distribution of conformations. We also see that such peptide-coated AuNCs can quickly adsorb onto TrxR1 and effectively target the region surrounding the protein's active site. Prior to contact with TrxR1, the distribution of the positively charged peptides becomes biased toward the acidic residues in the region around the enzyme's active site; the peptides extend toward the TrxR1 active site in a manner reminiscent of bacterial cilia reaching toward a positive stimulus.[45−48] After the AuNC contacts the protein surface, the peptides spread over surface of the protein and, through transient and cooperative interactions, facilitate stable binding with TrxR1. In addition, we find that the AuNC also satisfies a notable hydrophobic interaction involved in the Trx-TrxR1 activated complex, suggesting a mode through which AuNC binding specificity is achieved. We discuss the nature of all of these interactions in more detail below.

SYSTEM AND METHODOLOGY

As indicated by previous work,[49,50] the structure of our Au_{25} cluster is based on a centered icosahedral Au_{13} core, which is further capped by an exterior shell composed of 12 Au atoms. The Au_{25} cluster featured in the literature is encapsulated by 18 thiolate groups. In our system, the Au_{25} cluster is coated by nine tridecapeptides (sequence CCYGGPKKKRKVG). The peptide's eight residue C-terminal segment was adapted from the NLS (nucleus localization signal) peptide of simian virus 40 [SV40].[51,52] The mineralization sequence CCY (coupled to a GG linker) was added to the N-terminus of the NLS sequence: the dicysteine motif serves to anchor the tridecapeptides directly to the gold cluster center.[53] As previous experimental evidence indicates, such peptide-coated AuNCs can effectively penetrate cell membranes and bind to TrxR1.[38] In preparation for our initial TrxR1-free simulations, the coated AuNC was solvated in a cubic box with a dimension of 104 Å. Requisite numbers of sodium and chloride ions were then added to neutralize the system and to achieve a physiological ionic concentration of 150 mM; AuNC configurations were also studied in a solution of low ionic strength, to which only 45 chloride ions were added to neutralize the system. Following similar previous protocols,[39,54−58] the solvated system was first subjected to 50000 steps of energy minimization followed by 1000 ps of equilibration. A 200 ns production MD simulation was performed to investigate the solution structure of the peptide-coated AuNC.

The structure of TrxR1, in which the protein is bound to the cofactors FAD and NADPH, was obtained from the Protein Data Bank (PDB code 1H6V).[59] The homodimeric TrxR1 (with subunits A and B) possesses two redox centers: the first near the N-terminus (Cys59, Cys64) and the second adjacent to the C-terminus (Cys497, Sec498). Selenocysteine (Sec) is a cysteine residue analogue featuring a selenol group (-SeH) in place of cysteine's thiol moiety (-SH). It should be noted that the thioredoxin substrate interacts directly with the C-terminal redox center. In order to study the interactions between coated AuNCs and TrxR1, a AuNC was initialized at a distance of at least 20 Å from the model protein. The dimensions of the resulting system, containing ∼620 000 atoms, were 184 Å × 184 Å × 184 Å. Binding interactions between the AuNC and TrxR1 were studied in solutions of low ionic strength (wherein 31 chloride ions were added to neutralize the system) and at a physiological ionic concentration (0.15 M). After energy minimization, the system was equilibrated for 1000 ps; five configurations obtained from the last 500 ps of the equilibrium run were used as the initial configurations for five independent 50 ns simulations of binding between the AuNC and TrxR1.

All MD simulations were performed in the NPT ensemble at 1 bar and 300 K; the pressure and temperature of the system were maintained using the Parrinello−Rahman barostat and the velocity-rescaling thermostat, respectively. The OPLS-AA force field[60] and TIP3P water model[61] were used in this work. The particle-mesh Ewald (PME) method was employed to account for long-range electrostatic interactions, whereas a typical 10 Å cutoff distance was applied to calculations of short-range electrostatic and van der Waals energies. Standard periodic boundary conditions were applied throughout all simulations, which evolved with a time step of 1 fs. All the simulations were performed using the GROMACS 4.5.5 package.[62]

RESULTS

1. Structure of Peptide-Coated AuNC in Solution. First, we performed a 200 ns MD simulation to investigate the structural ensemble of the peptide-coated AuNC in solution. The radius of gyration (R_g) and root-mean-square deviation (RMSD) of the nanocluster computed over the course of the simulation are presented in Figure S1. In the chosen initial configuration (R_g = 2.05 nm), all peptides are fully extended and uniformly distributed. The overall R_g of the AuNC quickly decreases to around 1.56 nm in the first 15 ns of the observed dynamics (Figure S1), a change attributed to symmetry breaking and partial collapse within the peptide corona. Concurrently, the RMSD of the AuNC (to its initial configuration) significantly increases to around 1.49 nm (Figure S1), confirming that some structural arrangement indeed occurs inside the peptide corona. After the initial "collapse", the R_g of the AuNC still fluctuates to some extent (ranging between 1.5 and 1.65 nm, Figure S1), suggesting that configurational diversity and disorder persist over the course of our simulation. Selected configurations taken from these dynamics are shown in Figure 1.

We further characterize the distribution of peptides on the surface of the Au_{25} cluster by calculating the number of atoms that come in contact with the other peptides (Figure S2).

DOI: 10.1021/jacs.5b00888
J. Am. Chem. Soc. XXXX, XXX, XXX−XXX

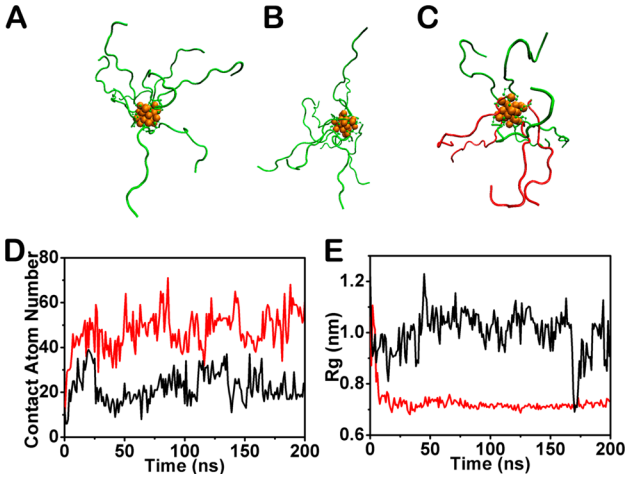

Figure 1. (A–C) Three typical structures of peptide-coated AuNCs. The gold atoms are shown in orange and the peptide chains are represented in green. (C) Two sets of adjacent peptides, highlighted in red, form reasonably persistent pairs in our simulations. (D) Representative contacting atom numbers observed, for single peptides D (red) and E (black) from the Supporting Information, with the rest of the peptide ensemble. (E) The radius of gyration for two representative peptides (now, peptides C (red) and E (black) from the Supporting Information).

Consider peptides D and E as representative examples (Figure S2D, S2E and Figure 1D). The average number of atoms in contact with peptide D is 49 (with a distance <4 Å, based on the last 175 ns of our trajectory), while the corresponding number for peptide E is less than half of that amount. This considerable difference in contact frequency clearly demonstrates a lack of uniformity within the AuNC's peptide coating. The contact number fluctuates considerably even within single peptides: in peptide E, for example, the number of contacting atoms varies between 8 and 37 throughout the middle portion of the trajectory (Figure 1D).

By tracking the R_g corresponding to each individual peptide (Figure S3), the structural diversity that appears within the peptide coating becomes more evident. The radii of many peptides (Figure S3B, S3E and Figure 1E) remain close to their values within the initial, fully extended configuration (~1.1 nm); on the other hand, the average R_g corresponding to peptide C is much smaller (0.72 nm). Accordingly, a varied ensemble of extended and collapsed peptides emerges over the course of the dynamics. In parallel to the contact number data, the radii of individual peptides undergo some fluctuation: the R_g of peptide E, for instance, jumps between 0.7 and 1.1 nm in the latter part of the simulation (Figure 1E).

A similarly disordered distribution of nanoparticle coating structures has also been observed in alkanethiol-coated gold clusters.[21−23] The tridecapeptide in our system, however, is unique in that it is highly charged: each coating molecule contains a motif of five consecutive, positively charged residues (i.e., KKKRK), meaning 45 positively charged residues are present in the peptide corona. On the other hand, the average number of anions in contact with the peptide corona (at distances smaller than 4 Å, based on the last 150 ns trajectory) is approximately 10: thus, only 20% of such positively charged residues are associated with counterion partners. The strong electrostatic repulsion among coating peptides is apparently insufficient to induce much homogeneity in coating structures. After all, given the inherent conformational flexibility of peptides and the complicated combinatorial nature of hydrogen bonds, we expect the entropy within the peptide ensemble to remain quite high. In several instances, we do see that adjacent peptides form persistent pairs stabilized by hydrogen bonds (with a persistence time of ~150 ns, as illustrated in Figure 1C). The distribution and structure of the peptide corona exhibit similar features at low ionic concentration: the average number of peptide-contacting anions is reduced to approximately 8, but this decreased ionic screening does not appear to affect the flexible structure of the peptide corona (Figure S1, S4–S6). As discussed below, this disordered and fluctuating peptide distribution plays important roles in the coated AuNC's interaction with TrxR1.

2. The Binding Process of AuNC to TrxR1 in Solution. As indicated by our previous work,[38] the peptide-coated AuNC interrogated here can effectively inhibit the activity of TrxR1 in the cytoplasm. We now study the binding of this AuNC to TrxR1 and investigate any prevailing modes of interaction between the enzyme and nanoparticle that might emerge. To reduce bias related to the initial conditions of our binding simulations, the AuNC and TrxR1 are started in a well-separated configuration: the AuNC is initialized at coordinates at least 2 nm away from the protein. The interactions between the AuNC and TrxR1 are then probed using 5 independent simulations, each lasting at least 50 ns in duration. To characterize the binding process, we track, in particular, the center of mass (COM) distance between the Au_{25} core of our AuNC and residues Cys497 and Sec498 of the active site of TrxR1 (subunit A), alongside a count of contacting atoms (with a distance smaller than 4 Å) between the AuNC and TrxR1. A representative binding event is characterized in Figure 2A.

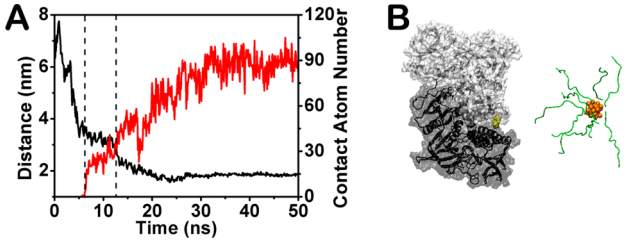

Figure 2. Important aspects of the binding process between AuNC and TrxR1. (A) The COM distance between the Au_{25} core of AuNC and Cys497, Sec498 of TrxR1 (black) and the number of contacting atoms between the AuNC and TrxR1 (red). (B) Representative snapshot taken from the binding process in Stage 1. Five out of nine peptides quickly shift toward TrxR1. The gold atoms, peptide chains, and Cys/Sec residues in the active site are depicted in orange, green and yellow, respectively.

The binding process between the AuNC and TrxR1 can roughly be represented in three stages. In Stage 1 (from t = 0 to 6 ns), the COM distance between Au_{25} core and the active site decreases rapidly to about 3.3 nm. We find that the motion of the coated AuNC is biased by apparent attraction to the protein, even when the separation is still large. Moreover, the AuNC exhibits a clear tendency to approach the region surrounding TrxR1's active site, which is largely negatively charged (more below). At the beginning of Stage 2 (around t = 6 ns), the AuNC comes into intransient contact with the protein; the COM distance further decreases to approximately 2.7 nm and the number of contacting atoms increases to about 35 over the next 7 ns of simulation time. From t = 13 to 50 ns

DOI: 10.1021/jacs.5b00888
J. Am. Chem. Soc. XXXX, XXX, XXX−XXX

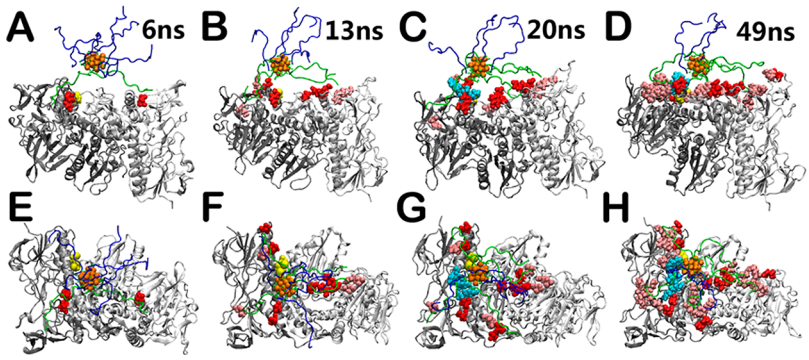

Figure 3. Representative snapshots taken from the binding process in Stages 2 and 3. (A–D) side view, (E–H) top view. The gold atoms and Cys/Sec residues in active site are represented in orange and yellow, the peptide chains in contact with protein are shown in green, while the other peptide chains are colored in blue. The negatively charged residues in direct contact with the AuNC are highlighted in red, and the other contacting residues are shown in pink. The Tyr residue of an AuNC coating peptide can fit into a pocket formed by the light blue residues around the active site of TrxR1.

(Stage 3), the COM distance slowly decreases to 1.8 nm, a separation close to the radius of the gold nanocluster; throughout that process, the contact number increases from 35 to 90 as the AuNC binds to the enzyme in earnest. A similar binding process was observed in the other four simulations at physiological ionic strength and in separate simulations at the low ionic concentration (Figure S7, S14, S15). Our observations suggest that when the distance between the center of mass (COM) of the AuNC and the TrxR1 active site falls below 6 nm, the approach of the AuNC starts to become directed. In terms of Smoluchowski rate theory,[63] the effective collision distance corresponding to the AuNC-TrxR1 association process should thus be approximately r_c = 6 nm. Employing measurements of the mean square displacement (MSD) of the AuNC in solution (Figure S8) to estimate the diffusion constant for the nanoparticle ($D = 2.1 \times 10^{-6}$ cm^2/s), we find that the association rate constant, $K_a = 4\pi r_c D$, between TrxR1 and our AuNC is approximately 9.5×10^9 M^{-1} s^{-1}. This simple calculation suggests that the binding of AuNCs to TrxR1 may proceed more efficiently than the association occurs in most protein–protein recognition systems.[64]

The directionally biased diffusion of the AuNC in Stage 1 is likely related to its electrostatic attraction to TrxR1, especially to the region surrounding the active site (i.e., the C-terminal redox center). The surface region within 2.5 nm of the active site contains at least 11 acidic residues—Asp231, Glu238, Glu241, Glu242, Glu387, Glu388, Glu400, Asp417, Asp491 (subunit A) and Glu103′, Glu122′ (subunit B)—meaning the neighborhood of the active site is mainly negatively charged (see Figure S9 for an illustration of the surface electrostatic potential). Cations in solution bind to this region with comparative modesty: the average number of positive contacting ions (at a distance smaller than 4 Å, based on the 6 ns Stage 1 trajectory) is 0.83. The largely unshielded, positively charged motifs contained within the tridecapeptide coating thus seem to experience electrostatic attraction to TrxR1, steering the diffusion of AuNC toward the protein active site.

During the nanoparticle's approaching process, the AuNC's coating peptides deviate toward the side of the cluster adjacent to TrxR1. In the early stages of the binding simulation described above, five of nine peptides quickly orient themselves to point toward TrxR1 (Figure 2B); other peptides follow suit as the nanocluster nears the enzyme's active site (Figure 3). The orientation of the peptide corona, thus, seems to be very sensitive to the external electric field created by the protein target.

To better illustrate the nature of this long-range attraction, we also conducted a simulation in which the heavy atoms of TrxR1 and the Au_{25} core are restrained to their initial positions but the peptide corona is free to adjust to its environment. We then compared the COM distances between the active site (Cys497-Sec498) and gold core, and between the active site and the peptide coating (Figure S10). Though the peptide coating is initially further from the binding pocket than the Au_{25} core, the separation between the peptide corona and the active site decreases quickly within the first 2.5 ns of simulation and overtakes the core COM distance. Such long-range attraction is also observed in the solution with lower ionic concentration (Figure S16).

The active site of TrxR1, thus, seems to exhibit long-range control over the distribution of coating peptides on the advancing gold nanocluster. The biased arrangement of peptides that results within the flexible, highly polarizable coating should only enhance the efficacy of the nanoparticle's approach. As a somewhat compelling visual analogy, the behavior of the peptide coating, upon approaching, resembles that of bacterial cilia in the presence of a stimulus. Cilia, of course, transmit signals transduced through the exceptionally sophisticated chemosensory system present in bacteria.[45−47] Nevertheless, this purely electrostatic attraction driven mechanism within the peptide-coated AuNC resembles bacteria's stimulus-driven approaching process.

After the AuNC touches the protein near the end of Stage 1 (i.e., around t = 6 ns), the diffusive motion of the nanocluster slows down and the number of contacts between the enzyme and the AuNC increases considerably. In contrast to Stage 1 (where interactions between the AuNC and TrxR1 are dominated by long-range electrostatic attraction), the dynamics in Stage 2 are defined by two coating peptides that directly contact the protein (Figure 3A, 3E). The association of these peptides is driven by nonbonded interactions with surface residues around the TrxR1 active site. By the end of Stage 2, the numbers of AuNC-protein salt bridges and hydrogen bonds have both increased to near double digit values (Figure S11). Such interactions, by tethering the nanocluster near the active site, also seem to facilitate the adsorption of additional peptide chains. The negatively charged residues surrounding the

DOI: 10.1021/jacs.5b00888
J. Am. Chem. Soc. XXXX, XXX, XXX–XXX

protein active site can thus serve as a "loading site" for AuNCs by attaching to the approaching nanoparticle and promoting further interaction.

At the end of Stage 2 (near t = 13 ns), another two coating peptides come into contact with the protein (Figure 3B, 3F); the number of contacting peptides increases to six over the course of Stage 3. The structural distribution of the peptide coating changes considerably after the nanoparticle comes into contact with TrxR1. Notably, the peptides appear to gradually spread over the protein surface, and, as a result, the contact surface area between the AuNC and TrxR1 increases markedly. By simulation's end, up to 45 residues belonging to TrxR1 are in direct contact with the AuNC (Figure 3D, 3H). The numbers of salt bridges and hydrogen bonds formed between the AuNC's peptide corona and TrxR1 also both increase, in concert, to respective averages of 8 and 19 (see Figure S11). In comparison, the number of salt bridges in the Trx-TrxR1 complex is only 5. The initial binding of this peptide-coated AuNC to TrxR1, featuring a plethora of electrostatically driven interactions, thus appears to be quite extensive. This strong association should facilitate the subsequent coordination with the SH/SeH groups present in the active site, disabling the principle reductive elements of TrxR1.

During the binding process, most coating peptides retain random-coil-like structures (Figure S12), and the configuration of the peptide coating adeptly adjusts to the distribution of negatively charged residues on the protein surface (Figure 3). Strikingly, up to ten acidic residues near the TrxR1 active site remain in direct contact with the AuNC until the end of the simulation. The observed binding mechanism is reminiscent of induced fit upon ligand binding, a mode of interaction facilitated by the flexibility and polarizability of the peptide corona. The action of the coating peptides in tethering the nanocluster to TrxR1 can once more be observed in the solution at low ionic strength (Figure S17, S18). Such behavior again evokes images of bacterial cilia: in a manner similar to the ciliary cooperation that anchors bacterial cells to substrates, the initial contact between the peptide coating and TrxR1 facilitates further interaction with proximal peptide chains.[48]

Ideas of cooperativity apply to interactions that occur later in the binding process, as well: even though the overall binding between the AuNC and protein is very stable, the binding of individual coating peptides is somewhat volatile (Figure S13; also see Figure S19 for the low ionic concentration case). For example, peptide E dissociates from TrxR1 at around t = 35 ns; near the same time, peptide B comes into contact with the protein and remains bound until the end of the simulation (Figure S13). The AuNC thus appears to bind to the protein in a fairly flexible manner, a binding mechanism characteristic of many other ligand−receptor complexes.

Though we have described the general nature of binding interactions observed in simulations, we have yet to propose a molecular mechanism that explains the binding specificity for this particular AuNC observed in experiments.[38] As indicated in the literature, the binding affinity of Trx for TrxR1 is mainly attributed to salt bridge interactions and the structural complementarities among select aromatic residues.[65] It should be noted that both types of interactions can, in fact, be satisfied by the peptide-coated AuNC as a TrxR1 ligand. Trx, for example, can form salt bridges with Glu103′ and Glu122′ of TrxR1 (subunit B); such salt bridge interactions can easily be realized with a bound AuNC. In the context of hydrophobic interactions, Trp31 of Trx fits nicely into a pocket formed by Asn107′, Gly110′, Ser111′, Trp114′ (subunit B). Interestingly, such fitting can also be observed with this AuNC: the N-terminal tyrosine (close to the Au_{25} core) within the tridecapeptide studied here can fit into a similar pocket formed by Gln106′, Asn107′, Ile109′, Gly110′, Ser111′, Asn113′, and Trp114′ (Figure 4A; also see Figure S20 for the low ionic concentration case). Adding to these complementary salt bridges and hydrophobic interactions, the concave surface region around the active site is conducive to enveloping the comparably sized Au_{25} core. At least 6 nonpolar residues are distributed throughout this concave region (i.e., Trp114′, Val118′, Trp407, Val413, Pro414 and Leu493; Figure 4B); such residues are well-placed for interaction with the nonpolar cysteine residues that anchor the peptide coating to the gold nanocluster core. All of these factors conspire to facilitate hydrophobic and charged binding interactions and generic shape matching with the peptide-coated AuNC. In summary, we have found that strong electrostatic interactions guide the peptide-coated AuNC into the Trx binding pocket, and we subsequently further reveal that a complement of charged, polar, and hydrophobic interactions secure the nanocluster within the TrxR1 active site.

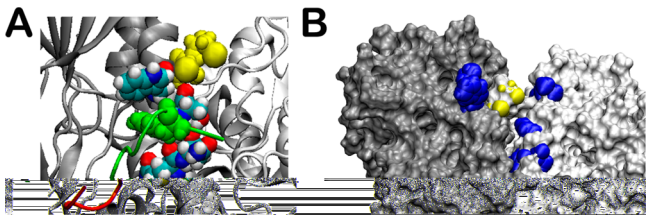

Figure 4. (A) The N-terminal Tyr residue of a coating peptide can fit into a pocket formed by the surface residues of TrxR1. The coating peptide (and its Tyr residue) is shown in green. (B) Several nonpolar residues (blue) are distributed throughout the concave region surrounding the active site of TrxR1 (yellow).

CONCLUSION

In this work, we have studied the structure and dynamical properties of a peptide-coated AuNC alongside its interactions with and binding to the redox-controlling enzyme TrxR1. We have found that the positively charged peptide coating on the nanocluster is flexible and susceptible to electrostatic attraction to the negatively charged surface region around protein's active site. After charge-directed diffusion leads to contact with TrxR1, the AuNC's peptide corona spreads over the protein surface and satisfies an array of interactions central to the binding mode favored within the active Trx-TrxR1 complex. It should be noted that the surface region surrounding the active site of TrxR2 is also negatively charged. Future work thus might be conducted to study the possible interactions between our AuNC and other isozymes, e.g., TrxR2 and TrxR3. Additionally, it is known that the structure of TrxR1 is modulated by the association of various cofactors;[59] it would also be interesting to investigate whether our AuNC can still bind to TrxR1 in the absence of such cofactor ligands.

Our results thus, for the first time, suggest a molecular mechanism by which this special peptide-coated AuNC binds to TrxR1 and inhibits its reductive activity. These simulations support the notion that the nanocluster in question binds strongly and with potential specificity to its intended target by satisfying critical interactions involved in protein recognition. In

DOI: 10.1021/jacs.5b00888
J. Am. Chem. Soc. XXXX, XXX, XXX−XXX

this regard, we feel that the featured AuNC might show promise as a therapeutic agent within its designed context. As supported by this work, the disordered quality of passivating and activating molecular coatings should likely be considered as a generic and early component of the design procedure. We hope, in general, that such findings help guide the development and application of nanoparticle-based therapies for the treatment of cancer and other human diseases.

■ ASSOCIATED CONTENT

Supporting Information

Supporting Figures S1−S20. The Supporting Information is available free of charge on the ACS Publications website at DOI: 10.1021/jacs.5b00888.

■ AUTHOR INFORMATION

Corresponding Authors

*ruhongz@us.ibm.com

*lijingyuan@ihep.ac.cn

Notes

The authors declare no competing financial interest.

■ ACKNOWLEDGMENTS

We thank Yaling Wang, Ru Liu and Qing Yuan for helpful discussions and acknowledge the Ministry of Science and Technology (MOST) 973 Program 2013CB933704, 2013CB932703 and National Natural Science Foundation of China (NSFC) Grants 21273240, 11204267 for funding. This work also is supported by the 100-Talent Project from the Chinese Academy of Science, the Natural Science Foundation of Hebei Province A2014203126 and the Program for the Outstanding Young Talents of Hebei Province.

■ REFERENCES

(1) Ghosh, P.; Han, G.; De, M.; Kim, C. K.; Rotello, V. M. *Adv. Drug Delivery Rev.* **2008**, *60*, 1307.

(2) Rosi, N. L.; Mirkin, C. A. *Chem. Rev.* **2005**, *105*, 1547.

(3) Peer, D.; Karp, J. M.; Hong, S.; FarokHzad, O. C.; Margalit, R.; Langer, R. *Nat. Nanotechnol.* **2007**, *2*, 751.

(4) Luedtke, W. D.; Landman, U. *J. Phys. Chem.* **1996**, *100*, 13323.

(5) Padovan-Merhar, O.; Lara, F. V.; Starr, F. W. *J. Chem. Phys.* **2011**, *134*, 244701.

(6) Le Guével, X.; Hötzer, B.; Jung, G.; Hollemeyer, K.; Trouillet, V.; Schneider, M. *J. Phys. Chem. C* **2011**, *115*, 10955.

(7) Van Lehn, R. C.; Alexander-Katz, A. *J. Phys. Chem. C* **2013**, *117*, 20104.

(8) Verma, A.; Stellacci, F. *Small* **2010**, *6*, 12.

(9) Negishi, Y.; Nobusada, K.; Tsukuda, T. *J. Am. Chem. Soc.* **2005**, *127*, 5261.

(10) Simms, G. A.; Padmos, J. D.; Zhang, P. *J. Chem. Phys.* **2009**, *131*, 214703.

(11) Xie, J. P.; Zheng, Y. G.; Ying, J. Y. *J. Am. Chem. Soc.* **2009**, *131*, 888.

(12) Xavier, P. L.; Chaudhari, K.; Verma, P. K.; Pal, S. K.; Pradeep, T. *Nanoscale* **2010**, *2*, 2769.

(13) Le Guevel, X.; Daum, N.; Schneider, M. *Nanotechnology* **2011**, *22*, 275103.

(14) Lin, C. A. J.; Yang, T. Y.; Lee, C. H.; Huang, S. H.; Sperling, R. A.; Zanella, M.; Li, J. K.; Shen, J. L.; Wang, H. H.; Yeh, H. I.; Parak, W. J.; Chang, W. H. *ACS Nano* **2009**, *3*, 395.

(15) Muhammed, M. A.; Verma, P. K.; Pal, S. K.; Kumar, R. C.; Paul, S.; Omkumar, R. V.; Pradeep, T. *Chem.—Eur. J.* **2009**, *15*, 10110.

(16) Retnakumari, A.; Setua, S.; Menon, D.; Ravindran, P.; Muhammed, H.; Pradeep, T.; Nair, S.; Koyakutty, M. *Nanotechnology* **2010**, *21*, 055103.

(17) Wei, H.; Wang, Z.; Yang, L.; Tian, S.; Hou, C.; Lu, Y. *Analyst* **2010**, *135*, 1406.

(18) Shang, L.; Dong, S.; Nienhaus, G. U. *Nano Today* **2011**, *6*, 401.

(19) Wen, F.; Dong, Y.; Feng, L.; Wang, S.; Zhang, S.; Zhang, X. *Anal. Chem.* **2011**, *83*, 1193.

(20) Wang, Y.; Cui, Y.; Zhao, Y.; Liu, R.; Sun, Z.; Li, W.; Gao, X. *Chem. Commun.* **2012**, *48*, 871.

(21) Lane, J. M. D.; Grest, G. S. *Phys. Rev. Lett.* **2010**, *104*, 235501.

(22) Guo, P.; Sknepnek, R.; Olvera de la Cruz, M. *J. Phys. Chem. C* **2011**, *115*, 6484.

(23) Ghorai, P. K.; Glotzer, S. C. *J. Phys. Chem. C* **2007**, *111*, 15857.

(24) Lin, J.; Zhang, H.; Chen, Z.; Zheng, Y. *ACS Nano* **2010**, *4*, 5421.

(25) Lin, J. Q.; Zheng, Y. G.; Zhang, H. W.; Chen, Z. *Langmuir* **2011**, *27*, 8323.

(26) Lee, O.-S.; Schatz, G. C. *J. Phys. Chem. C* **2009**, *113*, 2316.

(27) Seifpour, A.; Dahl, S. R.; Jayaraman, A. *Mol. Simul.* **2013**, 1.

(28) Lee, O. S.; Schatz, G. C. *Methods Mol. Biol.* **2011**, *726*, 283.

(29) Brancolini, G.; Kokh, D. B.; Calzolai, L.; Wade, R. C.; Corni, S. *ACS Nano* **2012**, *6*, 9863.

(30) Wang, L.; Li, J.; Pan, J.; Jiang, X.; Ji, Y.; Li, Y.; Qu, Y.; Zhao, Y.; Wu, X.; Chen, C. *J. Am. Chem. Soc.* **2013**, *135*, 17359.

(31) Fang, J.; Lu, J.; Holmgren, A. *J. Biol. Chem.* **2005**, *280*, 25284.

(32) Soderberg, A.; Sahaf, B.; Rosen, A. *Cancer Res.* **2000**, *60*, 2281.

(33) Berggren, M.; Gallegos, A.; Gasdaska, J. R.; Gasdaska, P. Y.; Warneke, J.; Powis, G. *Anticancer Res.* **1996**, *16*, 3459.

(34) Kahlos, K.; Soini, Y.; Saily, M.; Koistinen, P.; Kakko, S.; Paakko, P.; Holmgren, A.; Kinnula, V. L. *Int. J. Cancer* **2001**, *95*, 198.

(35) Berners-Price, S. J.; Filipovska, A. *Metallomics* **2011**, *3*, 863.

(36) Prast-Nielsen, S.; Cebula, M.; Pader, I.; Arner, E. S. *Free Radicals Biol. Med.* **2010**, *49*, 1765.

(37) Gao, X. US Patent: 2013; Vol. 8,383,919 B2.

(38) Liu, R.; Wang, Y.; Yuan, Q.; An, D.; Li, J.; Gao, X. *Chem. Commun.* **2014**, *50*, 10687.

(39) Eleftheriou, M.; Germain, R. S.; Royyuru, A. K.; Zhou, R. *J. Am. Chem. Soc.* **2006**, *128*, 13388.

(40) Li, X.; Li, J.; Eleftheriou, M.; Zhou, R. H. *J. Am. Chem. Soc.* **2006**, *128*, 12439.

(41) Krone, M. G.; Hua, L.; Soto, P.; Zhou, R. H.; Berne, B. J.; Shea, J.-E. *J. Am. Chem. Soc.* **2008**, *130*, 11066.

(42) Kang, S. G.; Huynh, T.; Xia, Z.; Zhang, Y.; Fang, H. P.; Wei, G. H.; Zhou, R. H. *J. Am. Chem. Soc.* **2013**, *135*, 3150.

(43) Xia, Z.; Das, P.; Shakhnovich, E. I.; Zhou, R. H. *J. Am. Chem. Soc.* **2012**, *134*, 18266.

(44) Das, P.; Kapoor, D.; Halloran, K. T.; Zhou, R. H.; Matthews, C. R. *J. Am. Chem. Soc.* **2013**, *135*, 1882.

(45) Silflow, C. D.; Lefebvre, P. A. *Plant Physiol.* **2001**, *127*, 1500.

(46) Bardy, S. L. *Microbiology* **2003**, *149*, 295.

(47) Wang, Q. F.; Suzuki, A.; Mariconda, S.; Porwollik, S.; Harshey, R. M. *EMBO J.* **2005**, *24*, 2034.

(48) Miyamura, S. *Cytologia* **2004**, *69*, 197.

(49) Heaven, M. W.; Dass, A.; White, P. S.; Holt, K. M.; Murray, R. W. *J. Am. Chem. Soc.* **2008**, *130*, 3754.

(50) Zhu, M.; Aikens, C. M.; Hollander, F. J.; Schatz, G. C.; Jin, R. *J. Am. Chem. Soc.* **2008**, *130*, 5883.

(51) Garcia-Santisteban, I.; Zorroza, K.; Rodriguez, J. A. *PLoS One* **2012**, DOI: 10.1371/journal.pone.0038570.

(52) Kobayashi, N.; Yamada, Y.; Yoshida, T. *Antimicrob. Agents Chemother.* **2006**, *50*, 1118.

(53) Wang, Y. L.; Cui, Y. Y.; Liu, R.; Wei, Y. T.; Jiang, X. G.; Zhu, H. R.; Gao, L.; Zhao, Y. L.; Chai, Z. F.; Gao, X. Y. *Chem. Commun.* **2013**, *49*, 10724.

(54) Zhou, R. H.; Huang, X. H.; Margulis, C. J.; Berne, B. J. *Science* **2004**, *305*, 1605.

(55) Liu, P.; Huang, X. H.; Zhou, R. H.; Berne, B. J. *Nature* **2005**, *437*, 159.

(56) Das, P.; King, J. A.; Zhou, R. *Proc. Natl. Acad. Sci. U. S. A.* **2011**, *108*, 10514.

(57) Zhou, R.; Das, P.; Royyuru, A. K. *J. Phys. Chem. B* **2008**, *112*, 15813.

DOI: 10.1021/jacs.5b00888
J. Am. Chem. Soc. XXXX, XXX, XXX−XXX

(58) Das, P.; Li, J.; Royyuru, A. K.; Zhou, R. *J. Comput. Chem.* **2009**, *30*, 1654.
(59) Sandalova, T.; Zhong, L.; Lindqvist, Y.; Holmgren, A.; Schneider, G. *Proc. Natl. Acad. Sci. U. S. A.* **2001**, *98*, 9533.
(60) Jorgensen, W. L.; Maxwell, D. S.; TiradoRives, J. *J. Am. Chem. Soc.* **1996**, *118*, 11225.
(61) Jorgensen, W. L.; Chandrasekhar, J.; Madura, J. D.; Impey, R. W.; Klein, M. L. *J. Chem. Phys.* **1983**, *79*, 926.
(62) Hess, B.; Kutzner, C.; van der Spoel, D.; Lindahl, E. *J. Chem. Theory Comput.* **2008**, *4*, 435.
(63) Northrup, S. H.; Erickson, H. P. *Proc. Natl. Acad. Sci. U. S. A.* **1992**, *89*, 3338.
(64) Chang, C. E.; Shen, T.; Trylska, J.; Tozzini, V.; McCammon, J. A. *Biophys. J.* **2006**, *90*, 3880.
(65) Fritz-Wolf, K.; Kehr, S.; Stumpf, M.; Rahlfs, S.; Becker, K. *Nat. Commun.* **2011**, *2*, 383.

DOI: 10.1021/jacs.5b00888
J. Am. Chem. Soc. XXXX, XXX, XXX−XXX